Int. J. Heat Mass Transfer. Vol. 30, No. 8, pp. 1637–1644, 1987
Printed in Great Britain

0017–9310/87 $3.00 + 0.00

Laminar natural-convection flow transitions in tilted three-dimensional longitudinal rectangular enclosures

H. Q. YANG and K. T. YANG
Department of Aerospace and Mechanical Engineering, University of Notre Dame, Notre Dame, IN 46556, U.S.A.

and

J. R. LLOYD
Department of Mechanical Engineering, Michigan State University, East Lansing, MI 48824, U.S.A.

(*Received* 5 *May* 1986 *and in final form* 26 *January* 1987)

Abstract—Numerical finite-difference calculations have been carried out to determine laminar flow transition and heat transfer characteristics in tilted three-dimensional rectangular differentially-heated longitudinal enclosures. The tilt angle at which heat transfer attains a local minimum corresponds to the transition from multicell to unicell flow structures. Numerical results have been found to agree very well with existing experimental data and observations. Simulation calculations have also been made to determine the effect of the lateral walls and it is found that the close proximity between the walls restrict flow development in that direction, thus reducing the overall heat transfer across the enclosure.

INTRODUCTION

NATURAL convection in tilted rectangular enclosures with differentially-heated side walls has attracted considerable attention because of many important applications including the design of solar collectors and double glazing windows. One of the features, as observed in experiments [1–3] and verified in numerical studies [4, 5], is associated with enclosures where, as the differentially-heated side walls are tilted from horizontal (heated-from-below situation, i.e. $\psi = 180°$ as shown in Fig. 1) to the vertical ($\psi = 90°$) position, there exists a critical angle corresponding to a local minimum heat transfer rate. This phenomenon is attributed to three-dimensional transition from a transverse-roll flow pattern to a two-dimensional unicellular flow pattern [1–5]. It should be noted that all the studies mentioned above deal with enclosures whose third dimension is large compared to the other two, and are often referred to as transverse enclosures. However, a different flow transition may be possible in longitudinal enclosures, the third dimension of which is much less than the other two. Basically, the mechanism of this transition is due to the interaction between thermal instability associated with the heated-from-below situation and the buoyancy-driven flows along the heated and cooled walls. By linear stability analyses, Davis [6] and Catton [7] have found that the preferred mode of convection is always some number of finite rolls with their axes parallel to the short side of the finite enclosure. This has been confirmed by the experiments of Stork and Müller [8]. Hence, on the basis of the geometry shown in Fig. 1, if $A_z(L/H)$ is greater than $A_x(W/H)$ it is expected that the finite rolls will have their axes parallel to the x-axis, as shown in Fig. 2(a). If A_x is less than unity, the shape of the roll section is narrow, while for A_x larger than unity it is square. However, for the case of A_z less than A_x the finite rolls will have axes parallel to the z-axis as shown in Fig. 2(b). On the other hand, when the enclosure in either case is in a vertical position ($\psi = 90°$), the fluid undergoes a unicellular circulation which aligns its axis in the z-direction as shown in Fig. 2(c). Thus, it is not difficult to see that this unicellular flow must be the result of complex flow transition from the thermal instability-driven rolls as ψ changes from 180° to 90°. The axes of the rolls change 90° for transverse enclosures ($A_z > A_x$), while for longitudinal enclosures ($A_z < A_x$) the axis remains the same. It can be expected that the case of $A_z = A_x$ will be even more complicated, since the convection mode at $\psi = 180°$ consists of two superimposed rolls at right angles, which is often called bimodal convection as discussed by Krishnamurti [9].

Three-dimensional numerical calculations have been carried out by Yang *et al.* [5] and by Ozoe *et al.* [4] to predict the critical angle for transverse enclosures ($A_z > A_x$) at several aspect ratios and Rayleigh numbers. It is shown in ref. [5] that the corresponding two-dimensional model is very adequate when the tilt angle ψ is increased from 0° to the critical angle ψ_c, while for $\psi > \psi_c$ the heat transfer rate according to this

NOMENCLATURE

A_x	aspect ratio, W/H
A_z	aspect ratio, L/H
c_p	dimensionless specific heat
c_{pm}	dimensionless mean specific heat
g_i	dimensionless gravitational acceleration vector, $i = 1, 2, 3$
H	height of enclosure (Fig. 1)
h	coefficient of heat transfer
k	dimensionless thermal conductivity
L	length of enclosure (Fig. 1)
Nu	Nusselt number, $hH/\bar{k}$
p	dimensionless static pressure
Ra	Rayleigh number, $\bar{\rho}\bar{g}\bar{\beta}(\bar{T}_H - \bar{T}_C)H^3/\bar{\mu}_R\bar{\alpha}_R$
S	source term
T	dimensionless temperature
u_i	dimensionless velocity, $i = 1, 2, 3$
W	width of enclosure (Fig. 1)
x, y, z	rectangular coordinates (Fig. 1)
$\Delta x, \Delta y, \Delta z$	calculation cell sizes
x_i	rectangular coordinates, $i = 1, 2, 3$.

Greek symbols

$\bar{\alpha}$	thermal diffusivity
β	volume expansion coefficient
δ_{ij}	Kronecker delta
μ	dimensionless dynamic viscosity
ρ	dimensionless density
Φ	dimensionless dissipation function
ψ	tilt angle (Fig. 1)
ψ_c	critical tilt angle.

Subscripts

C	cold wall
H	hot wall
i, j, k	coordinate indices
m	mean quantities
P, N, S, E, W	node designation of basic grid
R	reference quantities
t	time derivative.

Superscript

ˉ	dimensional quantities.

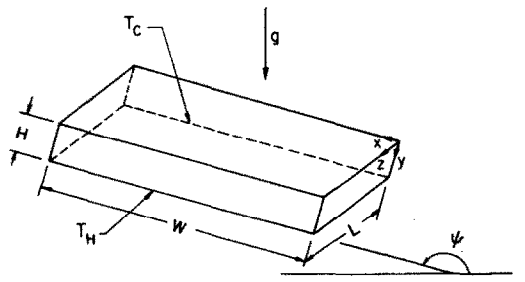

FIG. 1. Three-dimensional rectangular enclosure geometry.

model decreases further, in contrast to the increasing heat transfer obtained by the three-dimensional model which gives a local minimum at ψ_c. On the other hand, the unicellular flow pattern from the two-dimensional calculations persists until a higher angle is reached where the unicell breaks down into multiple rolls with axes in the same direction as the original unicell, unlike the three-dimensional transition of the unicellular flow pattern at ψ_c from the three-dimensional model calculations. Physically the two-dimensional transition can be accomplished by tilting the enclosure along the z-axis, as recently carried out experimentally by Symons and Peck [10] for a longitudinal enclosure. However, it should be noted that the two-dimensional model is only valid when the third dimension becomes very large so that the influence of the lateral walls vanishes. On the other hand, the longitudinal transition can only happen physically when the third dimension is small compared to the other two dimensions. It is therefore apparent that the two-dimensional model is incapable of describing the physical transition and heat transfer for longitudinal enclosures. The present numerical study is a continuation of studies given in ref. [5] and specifically deals with the flow transition in such longitudinal enclosures ($A_z < A_x$), and the results are compared directly with known experimental data.

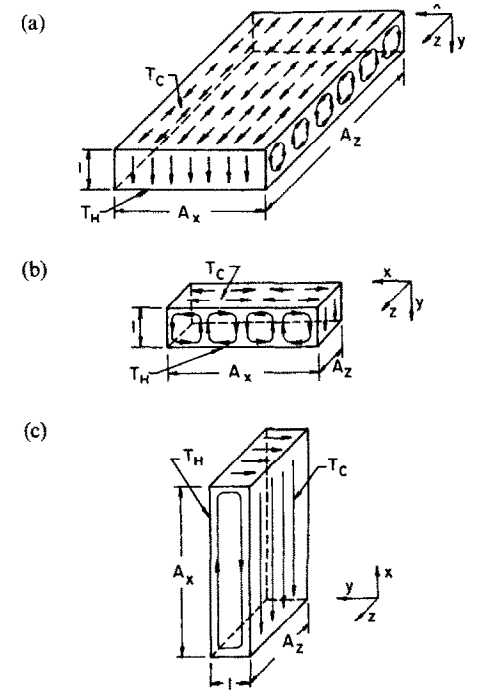

FIG. 2. Enclosure flow patterns: (a) transverse enclosure at $\psi = 180°$ ($A_z > A_x$); (b) longitudinal enclosure $\psi = 180°$ ($A_z < A_x$); (c) vertical enclosure at $\psi = 90°$.

GOVERNING EQUATIONS AND NUMERICAL SOLUTIONS

Figure 1 shows the geometry of a general three-dimensional rectangular enclosure. The surfaces at $y = 0$ and H are differentially heated with the cold surface at $y = 0$, and all the other surfaces are insulated. The aspect ratios which define the relative dimensions of the enclosure are $A_x = W/H$ and $A_z = L/H$. The working fluid is taken to be air. The equations governing the three-dimensional laminar natural convection process in enclosures are the conservation equations of mass, momentum and energy. By introducing the following definitions:

$$x_i = \frac{\bar{x}_i}{H}, \quad T = \frac{\bar{t}u_R}{H}, \quad g_i = \frac{\bar{g}_i H}{u_R^2}$$

$$u_i = \frac{\bar{u}_i}{u_R}, \quad T = \frac{\bar{T}}{T_R}, \quad p = \frac{\bar{p}}{\rho_R u_R^2} \tag{1}$$

$$\rho = \frac{\bar{\rho}}{\rho_R}, \quad c_{pm} = \frac{\bar{c}_{pm}}{c_{pR}}, \quad \mu = \frac{\bar{\mu}}{\rho_R u_R H},$$

$$k = \frac{\bar{k}}{\rho_R c_{pR} u_R H}$$

where all barred quantities are dimensional, subscript R refers to reference quantities, and $i = 1, 2, 3$. In the above equation, $\bar{x}_i$ is the rectangular coordinates, $\bar{t}$ the time variable, $\bar{g}_i$ the gravitational acceleration vector, $\bar{u}_i$ the velocity vector, $\bar{T}$ the temperature, $\bar{p}$ the static pressure, $\bar{\rho}$ the fluid density, $\bar{c}_{pm}$ the fluid mean specific heat, $\bar{\mu}$ the fluid viscosity, and $\bar{k}$ the fluid thermal conductivity. The governing conservation equations can now be written in dimensionless tensor forms as follows:

$$\rho_t + (\rho u_i)_{,i} = 0 \tag{2}$$

$$(\rho u_i)_t + (\rho u_i u_j)_{,j} = -p_{,i} - \rho g_i + \sigma_{ij,j} \tag{3}$$

$$(\rho c_{pm} T)_t + (\rho u_i c_{pm} T)_{,i} = (kT_{,i})_{,i} + \mu\Phi - \rho u_{i,i} \tag{4}$$

where subscript t denotes derivatives with respect to t. Furthermore, the dimensionless shear stress tensor σ_{ij}, c_{pm} and dissipation function Φ are in turn given respectively by

$$\sigma_{ij} = \mu(u_{i,j} + u_{j,i} - \tfrac{2}{3}\delta_{ij} u_{k,k}) \tag{5}$$

$$c_{pm} = \frac{1}{T-1}\int_1^T c_p \, dT \tag{6}$$

$$\Phi = 2(u_{i,j})^2 \delta_{ij} + [u_{i,j}(1-\delta_{ij})]^2 - \tfrac{2}{3}(u_{i,i})^2 \tag{7}$$

where δ_{ij} is the Kronecker delta. The variations of μ, k and c_p as functions of temperature are in accordance with that utilized in ref. [11]. The reference velocity u_R is chosen to be $0.3048\ \mathrm{m\,s^{-1}}$, and ρ_R and c_{pR} are evaluated at the cold wall temperature. The Boussinesq approximation is not invoked in the present study.

The governing equations are discretized by the control volume approach which insures the conservative characteristics to be satisfied in every cell and the whole calculation domain. A typical cell is shown in Fig. 3. The temperature, pressure, density and specific heat are evaluated at point P which is the center of the basic cell, while the flux quantities are evaluated at the surfaces of the cell, based on a staggered grid system. It is well known that discretizing first derivative terms leads to some inherent difficulties, because at a cell Peclet number larger than 2.0, the central difference scheme exhibits oscillatory or divergent behaviors, while the classical upstream scheme gives rise to serious artificial diffusion and low accuracy. In this study the QUICK (quadratic upstream interpolation for convection kinematics) scheme, originally suggested by Leonard [12, 13], is first extended to three-dimensional calculations and then utilized. This scheme has been shown to give good accuracy and stability [5].

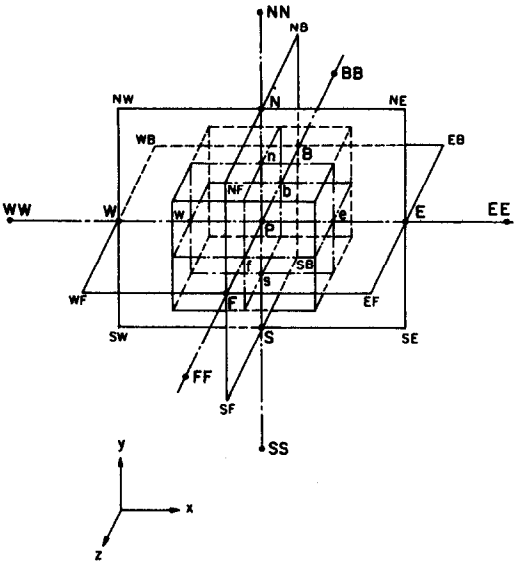

FIG. 3. Calculation cell.

The difficulty associated with the convective term is the evaluation of surface properties. Consider the temperature at the west control volume (Fig. 3) as an example.

By central difference, we have

$$T_w = 1/2(T_W + T_P). \tag{8}$$

By upstream difference, we have

$$\begin{aligned} T_w &= T_W \quad \text{if} \quad u_w > 0 \\ T_w &= T_P \quad \text{if} \quad u_w < 0 \end{aligned} \tag{9}$$

and by the QUICK scheme, the following may be written:

$$T_w = 1/2(T_W + T_P) - 1/8\,\mathrm{CURVN} + 1/24\,\mathrm{CURVT1} + 1/24\,\mathrm{CURVT2} \tag{10}$$

where CURVN is the stabilizing curvature term in the normal x-direction

$$\begin{aligned} \mathrm{CURVN} &= T_{WW} + T_P - 2T_W \quad \text{if} \quad u_w > 0 \\ &= T_W + T_E - 2T_P \quad \text{if} \quad u_w < 0 \end{aligned} \tag{11}$$

and CURVT1 and CURVT2 are the stabilizing curvature terms in the two transverse directions (y- and z-directions), as given by

$$\begin{aligned} \text{CURVT1} &= T_{NW}+T_{SW}-2T_W \quad \text{if} \quad u_w > 0 \\ \text{CURVT1} &= T_S+T_N-2T_P \quad \text{if} \quad u_w < 0 \\ \text{CURVT2} &= T_{WB}+T_{WF}-2T_W \quad \text{if} \quad u_w > 0 \\ \text{CURVT2} &= T_B+T_F-2T_P \quad \text{if} \quad u_w < 0. \end{aligned} \tag{12}$$

The final general finite-difference equation can then be written as

$$A_P T_P = A_W T_W + A_E T_E + A_S T_S + A_N T_N + A_B T_B + A_F T_F + S. \tag{13}$$

Here the source term S includes all the other terms at the neighboring points of P (such as $A_{NW}T_{NW}$, $A_{SW}T_{SW}$, $A_{BW}T_{BW}$, ...). Equation (13) is solved by an iterative tridiagonal matrix solver which has been described in our earlier enclosure studies [11, 14, 15] and will therefore not be repeated here.

RESULTS AND DISCUSSIONS

Symons and Peck [10] have given several sets of detailed experimental results for longitudinal enclosures. The dimensions of the enclosure are $H = 6.0$ cm, $W = 45.0$ cm and $L = 1.0$ cm, which result in $A_x = 7.5$ and $A_z = 1/6$. The temperature difference in the experiment is held at 30°C, while the air pressure inside the pressure vessel is adjusted to achieve different Rayleigh numbers. To match with the experimental conditions the initial pressure in the calculations is set such that the Rayleigh number is 3×10^5. The calculation domain is divided into 90 (x-direction) × 12 (y-direction) × 6 (z-direction) uniform rectangular control volumes or calculation cells with $\Delta x = \Delta y = 3\Delta z = 1/12$.

A three-dimensional numerical simulation has been carried out for this case, and the resulting flow patterns at different tilt angles are shown in Fig. 4. It is seen that at $\psi = 180°$, there are eight transverse cells with their axes parallel to the z-axis, and the cells are nearly square. At 165°, the cells on the far side are washed out due to the presence of an opposing gravitational force and the remaining cells, in which the gravitational force aids the circulation, become elongated, while those in which the gravity opposes the circulation are squeezed. As the enclosure is tilted to $\psi = 150°$, the first and third cells with the same sense of circulation near the axis of the tilt combine into a single cell, while the center or second cell is washed out. At an angle of 140°, the three cells on the far side in turn undergo a similar change to form a single cell and the cell in the middle becomes rather weak and finally vanishes at a tilt angle below 140°.

Also shown in Fig. 4 are the corresponding flow-visualization results of Symons and Peck [10]. The experimental and calculation results match very well at all tilt angles in terms of cell sizes and cell numbers. Nusselt number dependence on the tilt angle is given in Fig. 5. Curve (a) depicts the heat transfer characteristics across the longitudinal enclosure. Between angles 180° and 160°, the heat transfer rate is seen to be almost independent of the angle. The qualitative explanation of this phenomenon can be given in terms of the flow transition patterns (Fig. 4). In this range of tilt angles, the flow patterns change from eight cells to seven cells and intercellular upward convection remains strong. As the enclosure is further tilted to around 150°, the number of cells decrease to five and some of the cells become elongated. The reduction in cell number implies a reduction in intercellular convection (thermal instability effect). The resulting decrease in heat transfer, however, is still more important at this tilt angle than a slight increase in heat transfer due to the buoyancy force along the hot and cold walls (hydrodynamic effect). The net result is a further decrease in the overall heat transfer across the enclosure. Around a tilt angle of 140°, there are only three cells left with a very weak center cell as shown in Fig. 4. At an angle slightly below 140°, a unicellular flow pattern is formed, at which a local minimum heat transfer is observed. The characteristics of heat transfer at even smaller tilt angles are similar to those of a two-dimensional solution discussed in refs. [5, 15] even though the level of heat transfer rate is much lower in the present longitudinal enclosure case.

Symons and Peck's experimental heat transfer data [10] are also shown in Fig. 5. As discussed by them, the observed flow transition from multicell to unicell flow patterns (or vice versa) depends on the initial conditions. When the tilt angle is reduced through successive steady states from 180°, flow visualization indicates that the transition to unicell occurs close to $\psi = 140°$, which, as shown in Fig. 4, agrees well with the numerical simulation, which also starts at $\psi = 180°$. The numerical heat transfer results shown as curve (a) in Fig. 5 corresponds to the transition given in Fig. 4. However, the experimental heat transfer data of ref. [10] in Fig. 5 are that corresponding to a different sequence in which the transition is from a unicell flow pattern to multicell ones. In this case the transition, which is at the minimum heat transfer location, occurs at a tilt angle around 160°. Numerical simulation for this case has not been attempted in view of the fact that the corresponding flow visualization pictures are not indicated in ref. [10].

Numerical calculations have also been carried out to determine the influence of the lateral walls. The calculations are made for every 9° tilt angle in the regions of $0 \leqslant \psi \leqslant 108°$ and $153° \leqslant \psi \leqslant 180°$. However, tilt angles of 3° increments are used in the region $108° \leqslant \psi \leqslant 153°$ to anticipate possible sharp changes. For $A_x = 7.5$ and $A_z = 0.5$, the Nusselt number dependence on the tilted angle is shown by curve (b) in Fig. 5. The heat transfer is sharply increased because of the reduction in the physical restrain in the third direction. However, the variation does not have a sharp decrease

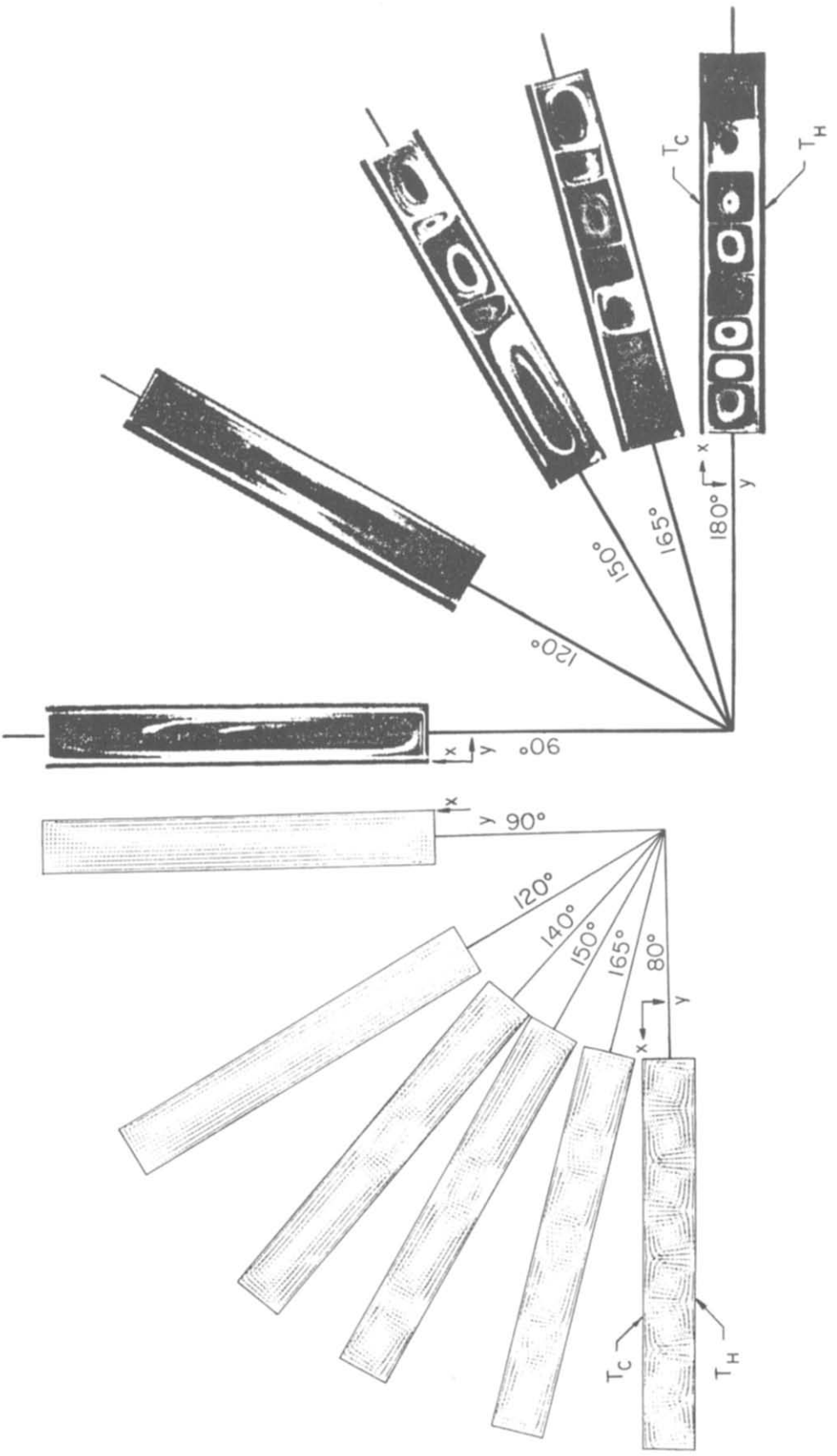

FIG. 4. Flow patterns in the x–y plane at $z = 0.5A_z$, $A_x = 7.5$, $A_z = 1/6$ and $Ra = 3 \times 10^5$.

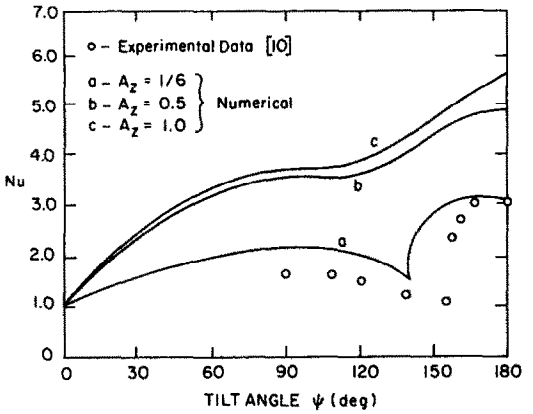

FIG. 5. Effect of tilt angle on Nusselt number, $A_x = 7.5$, $Ra = 3 \times 10^5$.

in the neighborhood of the minimum heat transfer point, as in the case of $A_z = 1/6$. Flow patterns at several locations of x are also plotted in Fig. 6. It is noted that the velocity vectors plotted in the lateral cross-sections (y–z plane) have a scale about a hundred times smaller than those given in the cross-sections in the x–y planes. This is also true in Fig. 7. It is seen in Fig. 6 that around 150° there is a development of a three-dimensional flow initiated at the two ends, similar to that found in ref. [5]. This lateral circulation increases the heat transfer, thus lessening the sharp drop in heat transfer close to the minimum heat transfer point. At the same time, the lateral flow also triggers an earlier transition to the unicell structure, as compared to the case of $A_z = 1/6$ in Fig. 4.

As A_z is increased further to 1.0, the three-dimensional flow is seen to initialize at an angle even closer to 180° (Fig. 7). It appears to play a dominant role in affecting the flow in the longitudinal or x–y plane. It is also interesting to note that the three-dimensional effect persists even at 90°. The corresponding heat transfer characteristics are shown as curve (c) in Fig. 5. Evidently, beyond $A_z = 0.5$, the lateral wall effect is no longer significant.

CONCLUDING REMARKS

A numerical finite-difference study based on the extended QUICK scheme has been conducted to determine laminar flow transition characteristics in tilted three-dimensional longitudinal air-filled rec-

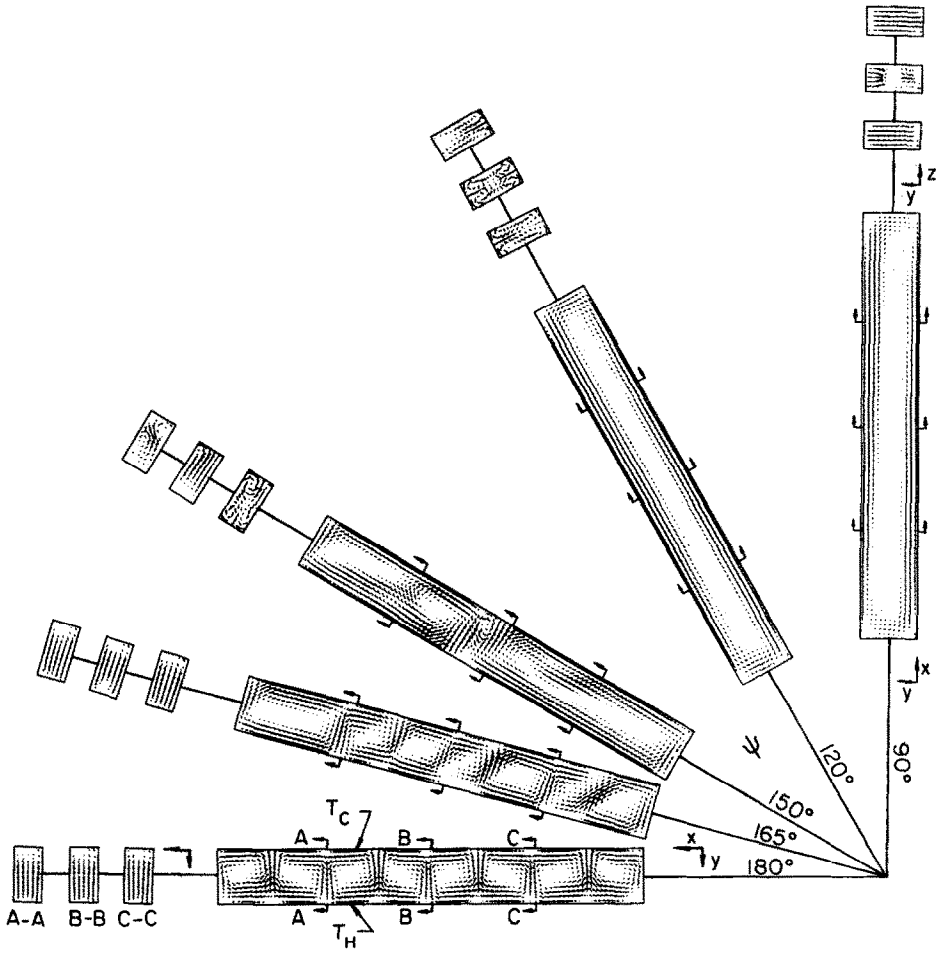

FIG. 6. Flow patterns at $z = 0.5A_z$, $A_x = 7.5$, $A_z = 0.5$ and $Ra = 3 \times 10^5$.

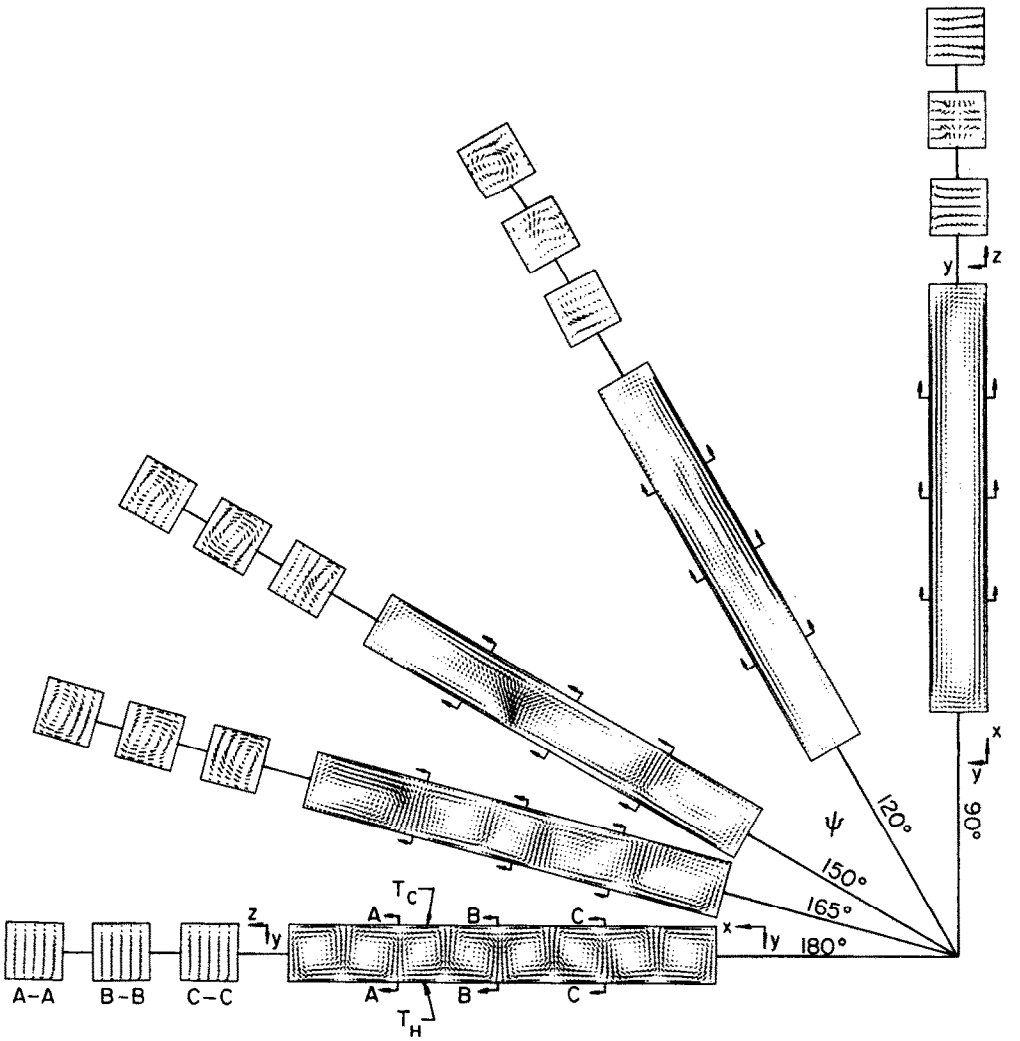

FIG. 7. Flow patterns at $z = 0.5A_z$, $A_x = 7.5$, $A_z = 1.0$ and $Ra = 3 \times 10^5$.

tangular enclosures. Tilt angles considered range from 180° (heated from below) to 90° (vertical enclosure) and to 0° (heat from top), with most calculations concentrated in the range between 180° and 90° in which flow transitions occur. Results have been obtained for a Rayleigh number of 3×10^5 and aspect ratios of $A_x = 7.5$ and $A_z = 1/6$ and are directly compared to existing experimental data. In addition, simulation calculations have also been carried out for $A_z = 0.5$ and 1.0 to determine the effect of lateral walls on the transition phenomena. The following conclusions can be drawn.

(1) For a longitudinal enclosure with small A_z, the axes of flow circulation within cells remain in the same direction when the enclosures are tilted from 180° to 0°, while it is known that for a transverse enclosure the axes undergo right angle changes [5].

(2) The presence of lateral walls in the third dimension dramatically affects both flow transition from multicell to unicell flow patterns and the rate of heat transfer. The location of such transition relative to the tilt angle corresponds to a minimum in the heat transfer rate. For a small A_z of 1/6 the transition is very abrupt, while for cases of $A_z = 0.5$ and 1.0, the transition is much more gradual.

(3) As the depth between the two lateral walls increases, the overall heat transfer across the enclosure also increases. However, this increase in the heat transfer rate is substantial for A_z changing from 1/6 to 0.5, while the increase is not substantial beyond $A_z = 0.5$. The relatively low heat transfer rates for $A_z = 1/6$ are due to the close proximity of the two lateral walls which restricts the development of any flow in the lateral direction.

(4) It is shown that the present numerical results simulate the experimental data of ref. [10] very well in terms of flow patterns in the entire range of the tilt angle and their transitions from multicell to unicell structures.

(5) The present numerical results complement those of ref. [5] for flow transitions in three-dimensional rectangular transverse enclosures, and it is believed that with the results obtained in the two studies, the

overall laminar flow transition phenomena in tilted rectangular enclosures that are differentially heated and the underlying physical mechanisms have now been substantially clarified.

Acknowledgement—The authors wish to acknowledge the support of the National Science Foundation under Grant CBT82-19158 to the University of Notre Dame, and the Computing Center of the University of Notre Dame.

REFERENCES

1. J. N. Arnold, I. Catton and D. K. Edwards, Experimental investigation of natural convection in inclined rectangular regions of differing aspect ratios, *J. Heat Transfer* **98,** 67–71 (1976).
2. H. Ozoe, H. Sayma and S. W. Churchill, Natural convection in an inclined rectangular channel at various aspect ratios and angles—experimental measurements, *Int. J. Heat Mass Transfer* **18,** 1425–1431 (1975).
3. W. M. M. Schinkel and C. J. Hoogendoorn, An interferometric study of the local heat transfer by natural convection in inclined air-filled enclosures, *Proc. 6th Int. Heat Transfer Conf.*, Toronto, Vol. 2, pp. 287–292 (1978).
4. H. Ozoe, K. Fujii, N. Lior and S. W. Churchill, Long rolls generated by natural convection in an inclined, rectangular enclosure, *Int. J. Heat Mass Transfer* **26,** 1427–1438 (1983).
5. H. Q. Yang, K. T. Yang and J. R. Lloyd, A flow transition in laminar buoyant flow in a three-dimensional tilted rectangular enclosure, *Proc. 8th Int. Heat Transfer Conf.*, San Francisco, Vol. 4, pp. 1495–1500 (1986).
6. S. H. Davis, Convection in a box: linear theory, *J. Fluid Mech.* **30,** 465–478 (1967).
7. I. Catton, The effect of insulating vertical walls on the onset of motion in a fluid heat from below, *Int. J. Heat Mass Transfer* **15,** 665–672 (1972).
8. K. Stork and U. Müller, Convection in boxes: experiments, *J. Fluid Mech.* **54,** 599–611 (1970).
9. R. Krishnamurti, Some further studies on the transition to turbulent convection, *J. Fluid Mech.* **60,** 285–303 (1973).
10. J. G. Symons and M. K. Peck, Natural convection heat transfer through inclined longitudinal slots, *J. Heat Transfer* **106,** 824–829 (1984).
11. Z. Y. Zhong, K. T. Yang and J. R. Lloyd, Variable property effects in laminar natural convection in a square enclosure, *J. Heat Transfer* **107,** 133–138 (1985).
12. B. P. Leonard, A stable and accurate modeling procedure based on quadratic-upstream interpolation, *Comput. Meth. Appl. Mech. Engng* **19,** 5–58 (1979).
13. B. P. Leonard, A convectively stable, third-order accurate finite-difference method for steady two-dimensional flow and heat transfer. In *Numerical Properties and Methodologies in Heat Transfer* (Edited by T. M. Shih), pp. 211–226. Hemisphere, Washington, D.C. (1983).
14. L. C. Chang, J. R. Lloyd and K. T. Yang, A finite-difference study of natural convection in complex enclosures, *Proc. 7th Int. Heat Transfer Conf.*, Munich, Vol. 2, pp. 183–188 (1982).
15. Z. Y. Zhong, K. T. Yang and J. R. Lloyd, Variable-property natural convection in tilted enclosures with thermal radiation. In *Numerical Methods in Heat Transfer* (Edited by R. W. Lewis and K. Morgan), Vol. III, pp. 195–224. Wiley, Chichester (1985).

TRANSITION LINEAIRE DE CONVECTION NATURELLE DANS DES ENCEINTES RECTANGULAIRES TRIDIMENSIONNELLES INCLINEES

Résumé—Des calculs numériques aux différences finies ont été faits pour déterminer la transition laminaire et les caractéristiques de transfert thermique dans des enceintes rectangulaires tridimensionnelles inclinées. L'angle d'inclinaison pour lequel le transfert de chaleur atteint un minimum local correspond à la transition de structure depuis l'écoulement multicellulaire vers celui unicellulaire. Des résultats numériques s'accordent très bien avec les données expérimentales et les observations existantes. Des calculs en simulation ont été faits pour déterminer l'effet des parois latèrales et on trouve que la proximité immédiate des parois restreint le développement de l'écoulement dans cette direction, réduisant ainsi le transfert thermique global à travers l'enceinte.

LAMINARE STRÖMUNG BEI NATÜRLICHER KONVEKTION IN GENEIGTEN DREIDIMENSIONALEN, LÄNGS VERLAUFENDEN, REICHTWINKLIGEN HOHLRÄUMEN

Zusammenfassung—Numerische Berechnungen mit dem Finite-Differenzen-Verfahren wurden durchgeführt, um die Charakteristik der laminaren Strömung und des Wärmeübergangs in geneigten dreidimensionalen rechtwinkligen, unterschiedlich beheizten, längs verlaufenden Hohlräumen zu bestimmen. Der Neigungswinkel, bei dem der Wärmeübergang ein lokales Minimum erreicht, korrespondiert mit dem Übergang von mehrzelliger zu einzelliger Strömungsstruktur. Die numerischen Ergebnisse stimmen sehr gut mit vorhandenen experimentellen Daten und Beobachtungen überein. Es wurden Simulationsrechnungen durchgeführt, um den Einfluß der Seitenwände zu bestimmen. Es stellt sich heraus, daß ein geringer Abstand zwischen den Wänden die Strömungsentwicklung in dieser Richtung einschränkt. Infolgedessen reduziert sich der gesamte Wärmedurchgang im Hohlraum.

ПЕРЕХОДНЫЕ РЕЖИМЫ ЛАМИНАРНОГО ЕСТЕСТВЕННО-КОНВЕКТИВНОГО ТЕЧЕНИЯ В НАКЛОННЫХ ТРЁХМЕРНЫХ ПРОДОЛЬНЫХ ПРЯМОУГОЛЬНЫХ ПОЛОСТЯХ

Аннотация—Методом конечных разностей исследован переходный режим ламинарного течения и теплообменные характеристики в наклонных трёхмерных прямоугольных продольных полостях с разной температурой боковых стенок. Угол наклона, при котором местный теплоперенос достигает минимальной величины, соответствует переходу от многоячеистой к одноячеистой структуре течения. Найдено, что численные результаты хорошо соответствуют имеющимся экспериментальным данным. Были также проведены модельные расчёты, с тем чтобы установить влияние боковых стенок. Найдено, что сближение стенок препятствует развитию течения в этом направлении, тем самым снижая теплоперенос через полость.